HHS Public Access

Author manuscript

Nature. Author manuscript; available in PMC 2014 May 07.

Published in final edited form as:

Nature. 2013 November 7; 503(7474): 111–114. doi:10.1038/nature12596.

Genetic identification of a neural circuit that suppresses appetite

Matthew E. Carter[1,2,§], **Marta E. Soden**[3,4], **Larry S. Zweifel**[3,4], and **Richard D. Palmiter**[1,2]

[1]Howard Hughes Medical Institute, University of Washington, Seattle, WA 98195 USA

[2]Department of Biochemistry, University of Washington, Seattle, WA 98195 USA

[3]Department of Pharmacology, University of Washington, Seattle, WA 98195 USA

[4]Department of Psychiatry, University of Washington, Seattle, WA 98195 USA

Abstract

Appetite suppression occurs following a meal and also during conditions when it is unfavorable to eat, such as during illness or exposure to toxins. A brain region hypothesized to play a role in appetite suppression is the parabrachial nucleus (PBN)[1-3], a heterogeneous population of neurons surrounding the superior cerebellar peduncle in the brainstem. The PBN is thought to mediate the suppression of appetite induced by the anorectic hormones amylin and cholecystokinin, as well as lithium chloride and lipopolysaccharide, compounds that mimic the effects of toxic foods and bacterial infections, respectively[4-6]. Hyperactivity of the PBN is also thought to cause starvation following ablation of orexigenic agouti-related peptide (AgRP) neurons in adult mice[1,7]. However, the identities of PBN neurons that regulate feeding are unknown, as are the functionally relevant downstream projections. Here we identify calcitonin gene-related peptide (CGRP)-expressing neurons in the outer external lateral subdivision of the PBN that project to the laterocapsular division of the central nucleus of the amygdala (CeAlc) as forming a functionally important circuit for the suppression of appetite. Using genetically-encoded anatomical, optogenetic[8], and pharmacogenetic[9] tools, we demonstrate that activation of PBelo CGRP neurons projecting to the CeAlc suppresses appetite. In contrast, inhibition of these neurons increases food intake in circumstances when mice do not normally eat and prevents starvation in adult AgRP neuron-ablated mice. Taken together, our data demonstrate that this neural circuit from the PBN to CeAlc mediates appetite suppression in conditions when it is unfavorable to eat. This neural circuit may provide targets for therapeutic intervention to overcome or promote appetite.

Corresponding author: Richard D. Palmiter, Ph.D. Department of Biochemistry, University of Washington Box 357350, 1705 NE Pacific Street, Seattle, WA 98195, palmiter@uw.edu.

[§]Present address: Department of Biology, Williams College, Williamstown, MA 01267, USA

Author Information: The authors declare no competing financial interests.

Supplementary Information: Supplementary Information includes Supplementary Figures 1-17, Supplementary Video 1, and Supplementary Statistical Analysis.

Author Contributions: M.E.C. and R.D.P. conceived of and designed the study. M.E.C. performed and analyzed histological and behavioral experiments, M.E.S. performed electrophysiology experiments, and R.D.P. generated *Calca*^{Cre} knock-in mice. L.S.Z. and R.D.P. provided equipment, reagents, and expertise. M.E.C. wrote the manuscript in collaboration with the other authors.

The PBN contains subpopulations of neurons that regulate taste[10,11], sodium intake[12,13], respiration[14], pain[15,16], thermosensation[17,18], and appetite suppression[1-3,7]. To identify a specific genetic marker for PBN neurons that suppress appetite, we analyzed expression of Fos, a surrogate marker of neuronal excitation, following genetic ablation of AgRP neurons or injection of lithium chloride (LiCl). AgRP neurons were ablated in mice expressing the human diphtheria toxin receptor (DTR) specifically in AgRP neurons (*Agrp*^{DTR} mice)[19]. Both AgRP neuron ablation (2 DT injections at 50 μg/kg, intramuscular) and LiCl injection (84 mg/kg, intraperitoneal) induced Fos expression in the outer external lateral subdivision of the PBN (PBelo; Supplementary Fig. 1). To identify a potential genetic marker for these neurons, we consulted the Allen Brain Explorer (http://mouse.brain-map.org)[20] and searched for genes enriched in the PBelo. The top candidate was *Calca*, the gene that encodes CGRP and calcitonin by alternative splicing[21]. Indeed, Fos expression in the PBN following ablation of AgRP neurons strongly overlapped with immunohistochemical detection of CGRP (Supplementary Fig. 2), similar to previous reports of coincident expression of Fos and CGRP following injection of LiCl or lipopolysaccharide (LPS)[6,22].

To control gene expression in these neurons, we generated a genetic knock-in mouse expressing Cre recombinase at the *Calca* locus (Supplementary Fig. 3). When these mice were crossed with Cre-dependent TdTomato reporter mice, ubiquitous red fluorescence was detected throughout the brain, likely due to transient Cre expression during development. However, injection of a Cre-dependent adeno-associated virus (AAV) carrying a mCherry reporter directly into the PBN region of adult *Calca*$^{Cre/+}$ mice (Fig. 1a) resulted in specific expression of mCherry in CGRP-positive neurons in the PBelo (Fig. 1b and Supplementary Figs. 4, 5).

To map activity in PBelo CGRP neurons, we compared virally targeted mCherry fluorescence with Fos following an array of environmental conditions that induce appetite suppression (see Supplementary Fig. 6 for specific paradigms used). In the lateral PBN, >80% of Fos expression co-localized with CGRP neurons following AgRP neuron ablation, intraperitoneal (i.p.) injection of LiCl, injection of LPS (Fig. 1c-h), or injection of the satiety hormones amylin or cholecystokinin (CCK; Supplementary Fig. 7a-d). In contrast, few Fos-positive neurons were observed in animals injected with saline (Fig. 1i,j), fasted for 24 h, or following aversive tail pinching (Supplementary Fig. 7e-h). Importantly, the percentage of CGRP neurons co-expressing Fos significantly correlated with the reduction in food intake relative to baseline conditions (Fig. 1k,l; see figure legends for P values and Supplementary Information for detailed statistical analyses). These results suggest that PBelo CGRP neurons are active during conditions in which appetite is suppressed but not in response to general adverse conditions.

To determine if transient stimulation of PBelo CGRP neurons is sufficient to reduce food intake, we unilaterally injected AAV carrying a Cre-dependent channelrhodopsin-2 transgene (AAV1 DIO ChR2-mCherry)[8] into the PBN of *Calca*$^{Cre/+}$ mice (Fig. 2a). Photostimulation reliably induced action potentials in mCherry-positive neurons in acute brainstem slices at multiple frequencies (20-40 Hz; Supplementary Fig. 8a) and 30 Hz photostimulation was sufficient to induce expression of Fos *in vivo* (Supplementary Fig. 8b,c). Stimulation of CGRP neurons *in vivo* for 5 min at 30 or 40 Hz (10-ms pulses)

significantly and reversibly suppressed food intake during both baseline conditions and also following a 24-h fast (Fig. 2b,c and Supplementary Fig. 8d), demonstrating that activating these neurons is sufficient to suppress food intake. Suppression of feeding following photostimulation was rapid (within 5-10 s; Supplementary Video 1) and reversible (mice typically resumed feeding within 5-10 min after photostimulation ceased). Importantly, stimulation at these frequencies did not impair movement or cause overt signs of distress (Supplementary Video 1).

To determine the effects of longer-term stimulation of PBelo CGRP neurons, we unilaterally transduced these neurons with AAV carrying a Cre-dependent hM_3Dq-mCherry[9,23] transgene (Fig. 2d). Stimulation of hM_3Dq with clozapine-N-oxide (CNO, 1 mg/kg) induced Fos expression (Supplementary Fig. 9) and suppressed food intake during both baseline conditions and following a 24-h fast (Fig. 2e,f). Chronic stimulation (once every 12 h for 4 d) resulted in a dramatic reduction in food intake and body weight (Fig. 2g,h), demonstrating that long-term activation of these neurons is sufficient to cause starvation.

To determine the effects of inhibiting PBelo CGRP neurons, we bilaterally transduced these neurons with AAV carrying a Cre-dependent hM_4Di-mCherry[9,23] transgene (Fig. 3a). In acute brainstem slices, bath infusion of CNO reversibly reduced the firing frequency of hM_4Di-expressing neurons to 24.98 ± 8.96% of baseline (Supplementary Fig. 10a,b). There was no change in baseline food intake or body weight following i.p. injection of CNO in either acute or chronic (once every 12 h for 4 d) conditions (Supplementary Fig. 11). However, inhibition of CGRP neurons with CNO decreased the suppression of appetite observed following injection of LiCl or LPS (Fig. 3b). Consistent with this observation, inhibition by hM_4Di also blocked the increase of Fos expression in the PBelo under these conditions (Supplementary Fig. 10c-f). Additionally, inhibition of CGRP neurons with CNO ameliorated appetite suppression following injection of amylin and CCK, although not to statistical significance (Fig. 3b). Because genetic ablation of AgRP neurons induces Fos expression in PBelo CGRP neurons and leads to starvation, we hypothesized that bilateral inhibition of CGRP neurons would prevent starvation in these animals. To test this hypothesis, we bred $Agrp^{DTR/+}$ mice with $Calca^{Cre/+}$ mice and bilaterally injected $Agrp^{DTR/+}/Calca^{Cre/+}$ offspring with AAV virus carrying Cre-dependent hM_4Di-mCherry. Indeed, chronic inhibition (injection of CNO every 12 h for 8 d) ameliorated the anorexia and prevented starvation following AgRP neuron ablation (Fig 3c,d). Taken together, these results demonstrate that inhibition of PBelo CGRP neurons increases food intake under conditions that normally suppress appetite.

To examine the relevant efferent projections of PBelo CGRP neurons, we simultaneously injected two AAV vectors carrying either Cre-dependent mCherry or Cre-dependent Synaptophysin-Green Fluorescent Protein (Syn-GFP) transgenes into the PBN of $Calca^{Cre/+}$ mice. We observed dense expression of mCherry- and GFP-positive fibers in the laterocapsular division of the central nucleus of the amygdala (CeAlc; Fig. 4a). This expression overlapped with immunohistochemical detection of CGRP in fiber terminals in the CeAlc (Fig. 4a) and is consistent with previous reports describing projections from the PBN to the central amygdala[16,24,25]. To a lesser degree, we also observed expression of mCherry and Syn-GFP in the bed nucleus of the stria terminalis (BNST; Supplementary Fig.

12). We observed sparse expression of mCherry and Syn-GFP in the lateral hypothalamus, medial thalamus, and within the dorsal PBN; expression was notably absent from previously described satiety centers, such as the arcuate nucleus[26] or paraventricular hypothalamus[27]. To confirm the specificity of projections from the PBelo to the CeAlc, we injected green fluorescent retrobeads into the CeAlc and AAV carrying Cre-dependent mCherry in the PBelo of *Calca*$^{Cre/+}$ mice. mCherry was expressed in >95% retrogradely-labeled green fluorescent neurons (Supplementary Fig. 13).

To demonstrate functional connectivity between the PBelo and the CeAlc, we transduced PBelo CGRP neurons with Cre-dependent ChR2-mCherry. *In* vivo photostimulation of either the PBelo or downstream projections in the CeAlc resulted in an increase in Fos expression within the CeAlc (Supplementary Fig. 14a-f). In acute brain slices, optical stimulation of ChR2-mCherry-positive fibers in the CeAlc resulted in excitatory postsynaptic currents (EPSCs, Fig. 4b and Supplementary Fig. 14g,h) and an increase in firing rate (Supplementary Fig. 14i) in CeAlc neurons (11 out of 25 cells showed an optically evoked response). The EPSCs and the increase in firing rate were blocked by bath application of the glutamate receptor antagonists CNQX (10 μM) and APV (50 μM), indicating that PBelo CGRP neurons form an excitatory synaptic connection with neurons of the CeAlc (Fig 4b and Supplementary Fig. 14g-i). To determine the effect of stimulating PBelo-to-CeAlc projections on food intake, we transduced PBelo CGRP neurons with ChR2-mCherry and implanted fiber optic cannulae above the CeAlc (Fig. 4c). Photostimulation of projections into the CeAlc for 5 min at 20-40 Hz significantly and reversibly suppressed food intake (Fig. 4d and Supplementary Fig. 15). In contrast, stimulation of PBelo projections to the BNST for 5 min had no significant effect on food intake (Supplementary Fig. 16). Taken together, these results indicate that direct projections from PBelo CGRP neurons to the CeAlc are sufficient to reduce food intake.

To determine the necessity of the PBelo-to-CeAlc projection in mediating appetite suppression, we bilaterally injected canine adenovirus (CAV2) carrying Cre recombinase into the CeAlc. CAV2 is capable of efficient retrograde transport[28] and therefore will express Cre in upstream PBelo neurons. In the same animals, we also bilaterally injected AAV carrying a Cre-dependent hM$_4$Di transgene into the PBN (Fig. 4e). Inhibition of PBN neurons with CNO decreased the suppression of appetite observed following injection of LiCl or LPS (Fig. 4f), demonstrating that activity in PBelo neurons projecting to the CeAlc is necessary for the normal suppression of appetite observed following injection of LiCl or LPS.

Taken together, these results demonstrate a neural circuit from CGRP-expressing neurons in the PBelo to the CeAlc that mediates appetite suppression. One of our observations was that inhibition of PBN neurons increased food intake when mice did not normally eat (Fig. 3b-d, Fig. 4f), but did not statistically increase food intake in baseline conditions (Supplementary Fig. 11) or following injection of amylin or CCK (Fig. 3b). These findings are consistent with those of Atasoy et al.[27], who did not find any effect on food intake following stimulation of inhibitory projections from AgRP neurons to the PBN. Perhaps inhibitory projections from AgRP neurons do not stimulate food intake in baseline conditions but do decrease the suppression of appetite when the PBN is most active. Thus, ablation of AgRP

neurons causes starvation in adult mice because of disinhibition in the PBelo[7]. Additionally, PBelo CGRP neurons may not mediate the ordinary, routine satiety experienced following a meal, but may mediate more severe forms of satiety experienced during severe overfeeding (gastric distention), illness, or other conditions in which it is unhealthy to eat such as dehydration or vertigo.

While it is well-established that multiple hypothalamic and brainstem nuclei coordinate appetite and satiety[26,29], this study demonstrates the involvement of downstream circuitry that may mediate the "unpleasant feeling" or discomfort that results from adverse conditions during which it is unfavorable to eat. Indeed, the CeAlc is known to process polymodal information about the internal and external bodily environment including adverse visceral stimuli[30]. Adding to previous results[1,7], we propose that PBelo CGRP neurons integrate visceral and energy balance information and communicate with the CeAlc to mediate extreme satiety and malaise (Supplementary Fig. 17).

Online Methods

Mice

All experiments were approved by the University of Washington Institutional Animal Care and Use Committee and were performed in accordance with the guidelines described in the U.S. National Institutes of Health *Guide for the Care and Use of Laboratory Animals*. We used exclusively heterozygous male *Calca*$^{Cre/+}$ and *Agrp*$^{DTR/+}$ mice backcrossed onto a C57Bl/6 background, aged 7-9 weeks at the start of experimental procedures and no more than 18 weeks at the end of experimental procedures. Prior to stereotaxic surgery, mice were group housed and maintained with rodent diet (Picolab, #5053) and water available *ad libitum* with a 12-h light-dark cycle at 22 °C. Following surgical procedures, mice were individually housed and maintained with a liquid diet (Vanilla Ensure, Abbot Laboratories) and water available *ad libitum*. We performed experiments on 3-4 experimental animals (e.g. animals transduced with ChR2, hM_3Dq, hM_4Di) and 3-4 control animals (e.g. animals only transduced with mCherry) at the same time to avoid differences in results between experimental sessions. Animals were randomly assigned to either the experimental or control group within each litter.

Generation of *Calca*^{Cre} mice

A 14 kb *BstB*1-*Pac*1 fragment was isolated from a C57Bl/6 mouse BAC clone. A unique *Sal*1 site was introduced at the initiation codon of *Calca* in exon 2 by PCR. Next, a 7 kb *Spe*1-*Sal*1 5′ fragment was cloned into a targeting vector containing a *frt*-flanked *PkgNeo* gene for positive selection and Pgk DTA and HSV-TK genes for negative selection. This was followed by insertion of a 3′ 7 kb *Sal*1-*Pac*1 fragment. The gene encoding the Cre-GFP fusion protein with an N-terminal myc-tag and nuclear localization signal was cloned into the unique *Xho*1 site adjacent to *frt-PgkNeo*. The targeting construct was linearized with *Asc*1 and electroporated into G4 hybrid (C57Bl/6 × Sv129) embryonic stem cells. Eighteen correctly targeted clones were identified out of 96 by Southern blot of *EcoRV* digested DNA using using a unique probe outside the targeting vector. Several of these clones gave good

chimeras when injected into C57Bl/6 hosts. One chimera was bred with FLPer (Rosa26-Flip recombinase) to remove the *frt-Pgk-Neo* gene.

Virus Production

Cre-dependent pAAV mCherry and ChR2-mCherry (driven by the Ef1α promoter) DNA plasmids were kindly provided by Dr. Karl Deisseroth and Cre-dependent pAAV hM_3Dq-mCherry and hM_4Di-mCherry (driven by the human synapsin promoter) DNA plasmids were kindly provided by Dr. Bryan Roth. pAAV Synaptophysin-GFP was generated by fusing the 3′ end of the mouse *Synaptophysin* coding region with the 5′ end of the *GFP* coding region. This sequence was then exchanged with mCherry in the pAAV mCherry plasmid to make the transgene Cre-dependent. Recombination-deficient AAV vectors were prepared in human embryonic kidney (HEK293T) cells with AAV1 coat serotype, purified by sucrose and CsCl gradient centrifugation steps, and resuspended in 1× Hanks Balanced Saline Solution (HBSS) at a titer of approximately 2×10^9 viral genomes/μl. CAV2 Cre was prepared in dog kidney (DK/E1-1) cells, purified by sucrose and CsCl gradient centrifugation steps, and resuspended in 1× HBSS at a titer of approximately 2.5×10^9 viral genomes/μl as described previously[31]. Viral aliquots were stored at −80 °C prior to stereotaxic injection.

Stereotaxic surgery

At the start of surgical procedures, mice were anesthetized with isofluorane and placed on a stereotaxic frame (David Kopf Instruments). Stereotaxic coordinates for the anterior-posterior plane were normalized using a correction factor [F = (Bregma – Lamda distance)/ 4.21] based on the coordinates of Paxinos and Franklin[32]. Virus was injected unilaterally (on the left side) or bilaterally as described in the text either in the PBN [anteroposterior (AP), −4.9 mm; mediolateral (ML), 1.4 mm; dorsoventral (DV), 3.8 mm] or the CeAlc (AP, −1.2 mm; ML, 2.6 mm; DV, 5.4 mm) at a rate of 0.2 μl/min for 2.5 min (0.5 μl total volume). Note that the viral injection coordinates target the most anterior aspect of the PBN, however, the virus diffuses posteriorly to hit all PBN subnuclei; this injection site improves the accuracy of injecting into the lateral PBN between the superior cerebellar peduncle (scp) and lateral wall of the pons. Also note that the presence of the scp fortuitously limits the spread of virus from the PBN region, thus preventing unintended transduction of other nearby *Calca*-expressing brain regions.

After viral injection, mice used for optogenetic experiments also received unilateral surgical implantation of a Mono Fiberoptic Cannula (Doric Lenses), either above the PBN (AP, −5.2 mm; ML, 1.6 mm; DV, 3.0 mm), CeAlc (AP, −1.2 mm; ML, 2.6 mm; DV, 5.4 mm) or BNST (AP, +0.14 mm; ML, 1.0 mm; DV, 4.0 mm). Cannulae were affixed to the skull with C&B Metabond (Parkell) and dental acrylic.

Slice electrophysiology

Coronal brain slices (250 μm) were prepared in an ice slush solution containing (in mM): 250 sucrose, 3 KCl, 2 $MgSO_4$, 1.2 NaH_2PO_4, 10 D-glucose, 25 $NaHCO_3$, 0.1 $CaCl_2$. Slices recovered for 1 hour at 34°C in artificial cerebral spinal fluid (ACSF) continually bubbled with O_2/CO_2 and containing (in mM): 126 NaCl, 2.5 KCl, 1.2 NaH_2PO_4, 1.2 $MgCl_2$ 11 D-

glucose, 18 $NaHCO_3$, 2 $CaCl_2$. Whole cell patch clamp recordings were made using an Axopatch 700B amplifier (Molecular Devices) with filtering at 1 KHz using 4-6 MΩ electrodes filled with an internal solution containing (in mM): 120 $CsMeSO_3$, 20 HEPES, 0.4 EGTA, 2.8 NaCl, 5 Mg-ATP, 0.5 Na-GTP, pH 7.2-7.4, 280 mOsm (for CeAlc single EPSC recordings) or: 135 $KMeSO_3$, 10 KCl, 10 HEPES, 0.1 EGTA, 2.8 NaCl, 5 Mg-ATP, 0.5 Na-GTP, pH 7.2-7.4, 280 mOsm (for PBN recordings and CeAlc high frequency stimulus recordings). ACSF at 32°C was continually perfused over slices at a rate of ~2 ml/min during recording.

For photostimulation experiments in the CeAlc, neurons surrounded by mCherry-positive fibers were selected for recording. For light-evoked EPSCs, neurons were held in voltage clamp at −70 mV, and EPSCs were stimulated by 10-ms pulses of blue laser light (single pulse at 0.1 Hz or 300 pulses at 30 Hz) using the same fiber optic as for the *in vivo* experiments, placed in the bath above the slice. Traces are averages of 15-20 sweeps for single EPSCs or averages of 3 sweeps for 30 Hz trains, collected before and 5 min after bath application of CNQX (10 μM) and APV (50 μM). For CeAlc current clamp recordings, the majority of CeAlc neurons had resting membrane potentials between −65 and −80 mV and did not fire action potentials spontaneously unless constant current was injected through the patch pipette to bring the cell closer to threshold. Trains of stimuli at 30 Hz were delivered as above.

For PBN ChR2 recordings, neurons identified by fluorescence were recorded in current clamp mode and trains of light pulses (1 ms) were delivered at the indicated frequencies for durations of 2 sec. For pharmacogenetic experiments, neurons expressing hM_4Di were identified by fluorescence. Cells that did not exhibit spontaneous firing were excluded. Neurons were recorded in current clamp mode in ACSF for a 5-min baseline period, followed by bath application of 3 μM CNO for 3 min, then washout with ACSF. Baseline firing rate was calculated from a 2-min window immediately prior to CNO application. CNO and washout firing rates were calculated from 2-min windows surrounding the maximum CNO effect and the maximum recovery period, respectively.

Food Intake Monitoring

For feeding assays, mice were individually housed in lickometer cages (Columbus Instruments) supplied with water and liquid diet (Vanilla Ensure, Abbot Laboratories) available *ad libitum*. Food and water ports were changed daily at the start of the dark cycle. The mice were allowed to acclimate to lickometer cages for 5 days and then baseline food intake was measured for an additional 5 days before experimental procedures. Acute food intake measurements (Fig. 2b,c,e,f; Fig. 3b; and Fig. 4d,f) occurred at the onset of the active period (lights off). Long-term measurements (Fig. 2g,h; Fig. 3c,d) occurred over a 24-h period with total food-intake and body weight measured approximately 6 h prior to the onset of the active period. Measurements were performed by an investigator (M.E.C.) with knowledge of the identity of the experimental versus control groups (*i.e.* without blinding).

Photostimulation

After a 14-day recovery period following surgery, mice were individually housed in lickometer cages with open cage tops. Fiber optic cables (1.5 m long, 200 μm diameter; Doric Lenses) coated with opaque heat-shrink tubing were firmly attached to the implanted fiber optic cannulae with zirconia sleeves (Doric Lenses). Mice were allowed at least 5 days to acclimate before experimental sessions. During photostimulation experiments, light pulse trains (10-ms pulses of various frequency; see text) were programmed using a waveform generator (Agilent Technologies, #33220A) that provided input to a blue light laser (473nm; LaserGlow). We adjusted the light power of the laser such that the light power exiting the fiber optic cable was 20 mW (160mW/mm^{-2}); using an online light transmission calculator for brain tissue[33] (www.stanford.edu/group/dlab/cgi-bin/graph/chart.php) we estimate the light power at the PBelo to be 36.2 mW/mm^{-2}. Note that this is probably a high estimation because some light is probably lost at the interface between the fiber optic cable and the implanted fiber optic cannula. After the completion of photostimulation experiments, mice were perfused and the approximate locations of fiber tips were identified based on the coordinates of Paxinos and Franklin[32].

Pharmacological injections

Pharmacological compounds were prepared in sterile 0.9% saline and stored at −20 °C prior to use. Diptheria toxin (DT) was injected intramuscularly and all other compounds were administered intraperitoneally as described in Supplementary Fig. 6 Compounds included amylin (10 μg/kg; Bachem, #H-9475), CCK-8 (10 μg/kg; Bachem, #H-2080), CNO (1 mg/kg; Sigma, #C0832), Diphtheria toxin (50 μg/kg; List Biologicals, #150), LiCl (84 mg/kg; 0.20 M at 10 ml/kg; Fisher, #L121), and LPS, *Salmonella typhimurium* (50 μg/kg; Calbiochem, #437650).

Histology

Mice were anesthetized with buprenorphine and perfused transcardially with 1× PBS, pH 7.4, followed by 4% paraformaldehyde in PBS. The brains were extracted, allowed to postfix overnight in the same fixative at 4 °C, and cryoprotected in 30% sucrose dissolved in 1× PBS for an additional 24 h at 4 °C. Each brain was sectioned at 30 μm on a cryostat (Leica Microsystems) and collected in cold 1× PBS.

For immunohistochemistry experiments, sections were washed three times in PBS with 0.2% Triton X-100 (PBST) for 10 min at room temperature. Sections were then incubated in a blocking solution composed of PBST with 3% Normal Donkey Serum (Jackson ImmunoResearch, #017-000-121) for 1 h. For primary antibody exposure, sections were incubated in rabbit anti-c-Fos (1:2000, Calbiochem, #PC38), rabbit anti-GFP (1:1000, Invitrogen, #A11122) and/or goat anti-CGRP (1:500, Abcam, #ab36001) in blocking solution at 4 °C for ∼20 h. After 3 × 10-min washes in PBST, sections were incubated in Alexa Fluor 594 donkey anti-goat IgG (1:200, Jackson Immunoresearch, #705-858-147), Alexa Fluor 488 donkey anti-goat IgG (1:200, Jackson Immunoresearch, #705-485-147), DyLight 405 donkey anti-goat (1:200, Jackson Immunoresearch, #705-475-147), and/or Alexa Fluor 488 donkey anti-rabbit IgG (1:200 Jackson Immunoresearch, #711-545-152) in

block solution for 1 h at room temperature. Finally, sections were washed three times in 1× PBS.

Sections were mounted in PBS onto SuperFrost Plus glass slides (VWR, #48311-703) and coverslipped with Dapi Fluoromount-G (Southern Biotech, #0100-20). Slides were stored in the dark at 4 °C prior to microscopy and image acquisition.

Quantification of colocalization of Fos and mCherry in the PBN (Fig 1-j and Supplementary Fig. 7) was performed on adjacent sections from approximately Bregma –4.90 to –5.50 (exactly 21 sections per mouse). Quantification of Fos in the CeAlc (Supplementary Fig. 14a-f) was performed on adjacent sections from approximately Bregma −1.14 to −1.26 (exactly 5 sections per mouse). A Fos-positive cell was considered located in the CeAlc if it was within the field of mCherry fluorescence within that particular section. All quantification analysis was performed by an investigator (M.E.C.) blinded to the identity of the conditions used to induce Fos.

Microscopy

Fluorescent and brightfield images were collected on either a Nikon upright epifluorescent microscope with QImaging Camera (Fig 1a,b; Fig. 4a; Supplementary Fig. 1) or a Zeiss LSM 510 Meta confocal microscope. Images were minimally processed using Photoshop CS5 (Adobe Systems) to enhance brightness and contrast for optimal representation of the data. Low magnification brightfield images (Fig. 1a, Fig. 4a, and Supplementary Fig. 4) were montaged together to produce a single coronal section. All digital images were processed in the same way between experimental conditions to avoid artificial manipulation between different datasets.

Statistics

We used an online power and sample size calculator to determine an effective sample size for statistical comparisons[34] (http://homepage.cs.uiowa.edu/~rlenth/Power/). Assuming a standard deviation of 1.0 and a significance level of 0.05, this calculator shows that with 8 mice per group we had an 80% confidence of achieving statistical significance between means of 1.5 fold with a two-tailed Student's t-test. We excluded an animal from data analysis if flagged by a University of Washington veterinarian for health reasons during the experimental period or if post-hoc histological analysis showed no viral transduction as indicated by an absence of mCherry fluorescence.

All data were analyzed using Prism 6.0 (GraphPad Software) as described in the text and Supplementary Statistical Analysis. Data were exported into Illustrator CS5 (Adobe Systems) for preparation of figures.

Supplementary Material

Refer to Web version on PubMed Central for supplementary material.

Acknowledgments

We thank Bryan Roth for hM_3Dq-mCherry and hM_4Di-mCherry constructs, and Karl Deisseroth for mCherry and ChR2-mCherry constructs. Elyse Allen, Jesse Resnick, Matthew Soleiman, and Stephanie Padilla assisted with histology, Elyse Allen and Aundrea Rainwater assisted with animal husbandry, and Jay Shulkin provided expert suggestions and advice. We thank members of the Palmiter and Zweifel labs for critical feedback on the manuscript. M.E.C. is funded by a fellowship from the Hilda and Preston Davis Foundation. L.S.Z. is funded by a grant from the NIH (R01MH094536). R.D.P is supported in part by grants from the NIH (DA024908) and the Klarman Family Foundation.

References

1. Wu Q, Clark MS, Palmiter RD. Deciphering a neuronal circuit that mediates appetite. Nature. 2012; 483:594–597. [PubMed: 22419158]
2. Becskei C, Grabler V, Edwards GL, Riediger T, Lutz TA. Lesion of the lateral parabrachial nucleus attenuates the anorectic effect of peripheral amylin and CCK. Brain Res. 2007; 1162:76–84. [PubMed: 17617389]
3. DiPatrizio NV, Simansky KJ. Activating parabrachial cannabinoid CB1 receptors selectively stimulates feeding of palatable foods in rats. The Journal of neuroscience. 2008; 28:9702–9709. [PubMed: 18815256]
4. Yamamoto T, et al. C-fos expression in the rat brain after intraperitoneal injection of lithium chloride. Neuroreport. 1992; 3:1049–1052. [PubMed: 1337282]
5. Elmquist JK, Scammell TE, Jacobson CD, Saper CB. Distribution of Fos-like immunoreactivity in the rat brain following intravenous lipopolysaccharide administration. J Comp Neurol. 1996; 371:85–103. [PubMed: 8835720]
6. Paues J, Mackerlova L, Blomqvist A. Expression of melanocortin-4 receptor by rat parabrachial neurons responsive to immune and aversive stimuli. Neuroscience. 2006; 141:287–297. [PubMed: 16730913]
7. Wu Q, Boyle MP, Palmiter RD. Loss of GABAergic signaling by AgRP neurons to the parabrachial nucleus leads to starvation. Cell. 2009; 137:1225–1234. [PubMed: 19563755]
8. Yizhar O, Fenno LE, Davidson TJ, Mogri M, Deisseroth K. Optogenetics in neural systems. Neuron. 2011; 71:9–34. [PubMed: 21745635]
9. Armbruster BN, Li X, Pausch MH, Herlitze S, Roth BL. Evolving the lock to fit the key to create a family of G protein-coupled receptors potently activated by an inert ligand. Proc Natl Acad Sci U S A. 2007; 104:5163–5168. [PubMed: 17360345]
10. Rosen AM, Victor JD, Di Lorenzo PM. Temporal coding of taste in the parabrachial nucleus of the pons of the rat. J Neurophysiol. 2011; 105:1889–1896. [PubMed: 21307316]
11. Tokita K, Boughter JD Jr. Sweet-bitter and umami-bitter taste interactions in single parabrachial neurons in C57BL/6J mice. J Neurophysiol. 2012; 108:2179–2190. [PubMed: 22832571]
12. Geerling JC, Loewy AD. Sodium deprivation and salt intake activate separate neuronal subpopulations in the nucleus of the solitary tract and the parabrachial complex. J Comp Neurol. 2007; 504:379–403. [PubMed: 17663450]
13. Geerling JC, et al. FoxP2 expression defines dorsolateral pontine neurons activated by sodium deprivation. Brain Res. 2011; 1375:19–27. [PubMed: 21108936]
14. Chamberlin NL, Saper CB. Topographic organization of respiratory responses to glutamate microstimulation of the parabrachial nucleus in the rat. The Journal of neuroscience. 1994; 14:6500–6510. [PubMed: 7965054]
15. Hermanson O, Blomqvist A. Subnuclear localization of FOS-like immunoreactivity in the rat parabrachial nucleus after nociceptive stimulation. J Comp Neurol. 1996; 368:45–56. [PubMed: 8725293]
16. Richard S, Engblom D, Paues J, Mackerlova L, Blomqvist A. Activation of the parabrachio-amygdaloid pathway by immune challenge or spinal nociceptive input: a quantitative study in the rat using Fos immunohistochemistry and retrograde tract tracing. J Comp Neurol. 2005; 481:210–219. [PubMed: 15562506]

17. Nakamura K, Morrison SF. A thermosensory pathway that controls body temperature. Nature neuroscience. 2008; 11:62–71. [PubMed: 18084288]
18. Nakamura K, Morrison SF. A thermosensory pathway mediating heat-defense responses. Proc Natl Acad Sci U S A. 2010; 107:8848–8853. [PubMed: 20421477]
19. Luquet S, Perez FA, Hnasko TS, Palmiter RD. NPY/AgRP neurons are essential for feeding in adult mice but can be ablated in neonates. Science. 2005; 310:683–685. [PubMed: 16254186]
20. Ng L, et al. An anatomic gene expression atlas of the adult mouse brain. Nature neuroscience. 2009; 12:356–362. [PubMed: 19219037]
21. Jacobs JW, et al. Calcitonin messenger RNA encodes multiple polypeptides in a single precursor. Science. 1981; 213:457–459. [PubMed: 6264603]
22. Paues J, Engblom D, Mackerlova L, Ericsson-Dahlstrand A, Blomqvist A. Feeding-related immune responsive brain stem neurons: association with CGRP. Neuroreport. 2001; 12:2399–2403. [PubMed: 11496118]
23. Krashes MJ, et al. Rapid, reversible activation of AgRP neurons drives feeding behavior in mice. J Clin Invest. 2011; 121:1424–1428. [PubMed: 21364278]
24. D'Hanis W, Linke R, Yilmazer-Hanke DM. Topography of thalamic and parabrachial calcitonin gene-related peptide (CGRP) immunoreactive neurons projecting to subnuclei of the amygdala and extended amygdala. J Comp Neurol. 2007; 505:268–291. [PubMed: 17879271]
25. Schwaber JS, Sternini C, Brecha NC, Rogers WT, Card JP. Neurons containing calcitonin gene-related peptide in the parabrachial nucleus project to the central nucleus of the amygdala. J Comp Neurol. 1988; 270:416–426. 398–419. [PubMed: 2836477]
26. Elmquist JK, Coppari R, Balthasar N, Ichinose M, Lowell BB. Identifying hypothalamic pathways controlling food intake, body weight, and glucose homeostasis. J Comp Neurol. 2005; 493:63–71. [PubMed: 16254991]
27. Atasoy D, Betley JN, Su HH, Sternson SM. Deconstruction of a neural circuit for hunger. Nature. 2012; 488:172–177. [PubMed: 22801496]
28. Soudais C, Laplace-Builhe C, Kissa K, Kremer EJ. Preferential transduction of neurons by canine adenovirus vectors and their efficient retrograde transport in vivo. Faseb J. 2001; 15:2283–2285. [PubMed: 11511531]
29. Gao Q, Horvath TL. Neurobiology of feeding and energy expenditure. Annu Rev Neurosci. 2007; 30:367–398. [PubMed: 17506645]
30. Neugebauer V, Li W, Bird GC, Han JS. The amygdala and persistent pain. Neuroscientist. 2004; 10:221–234. [PubMed: 15155061]
31. Kremer EJ, Boutin S, Chillon M, Danos O. Canine adenovirus vectors: an alternative for adenovirus-mediated gene transfer. J Virol. 2000; 74:505–512. [PubMed: 10590140]
32. Paxinos, G.; Franklin, KBJ. The mouse brain in stereotaxic coordinates. 4th. ElsevierAcademic Press; Amsterdam ; Boston: 2013.
33. Aravanis A, Wang LP, Zhang F, Meltzer L, Mogri M, Schneider MB, Deisseroth K. An optical neural interface: *in vivo* control of rodent motor cortex with integrated fiberoptic and optogenetic technology. J Neural Eng. 2007; 4:S143–156. [PubMed: 17873414]
34. Lenth RV. Some practical guidelines for effective sample size determination. The Am Stat. 2001; 55:187–193.

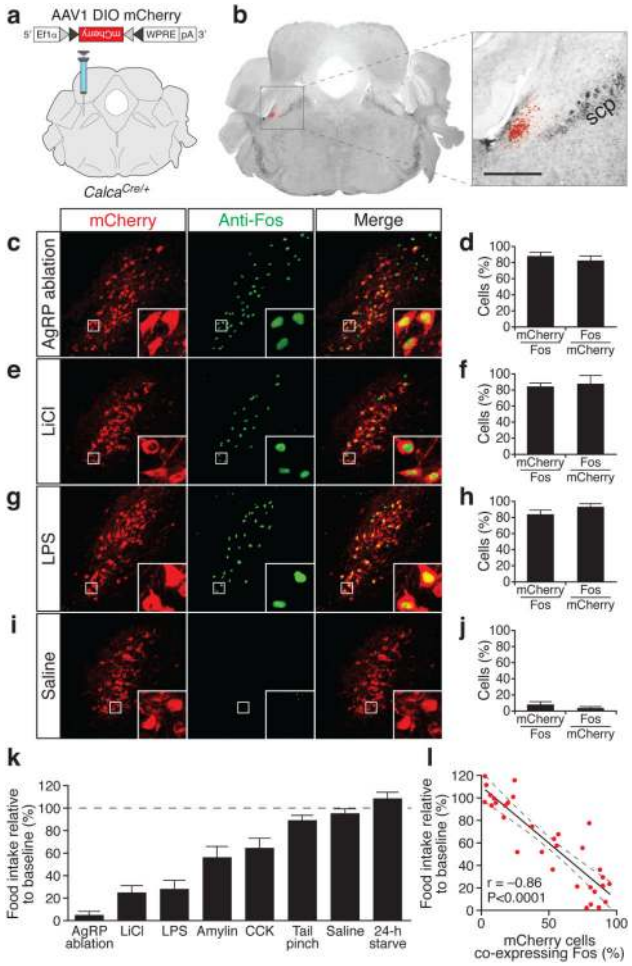

Figure 1. Co-localization of PBelo CGRP neurons with Fos following conditions that reduce food intake

a, AAV carrying a Cre-dependent mCherry reporter injected into the PBN. Grey triangles and black triangles represent loxP and lox2722 sites, respectively. **b,** mCherry expression in the PBelo. scp, superior cerebellar peduncle; scale bar, 500 μm. **c-j,** Representative histological examples and quantification of coincidence of mCherry and Fos expression. **k,** Degree to which various conditions reduce food intake. **l,** Appetite suppression correlates with the percentage of PBelo CGRP neurons expressing Fos. Dashed lines represent 95% confidence intervals. See Supplementary Information for statistical analysis.

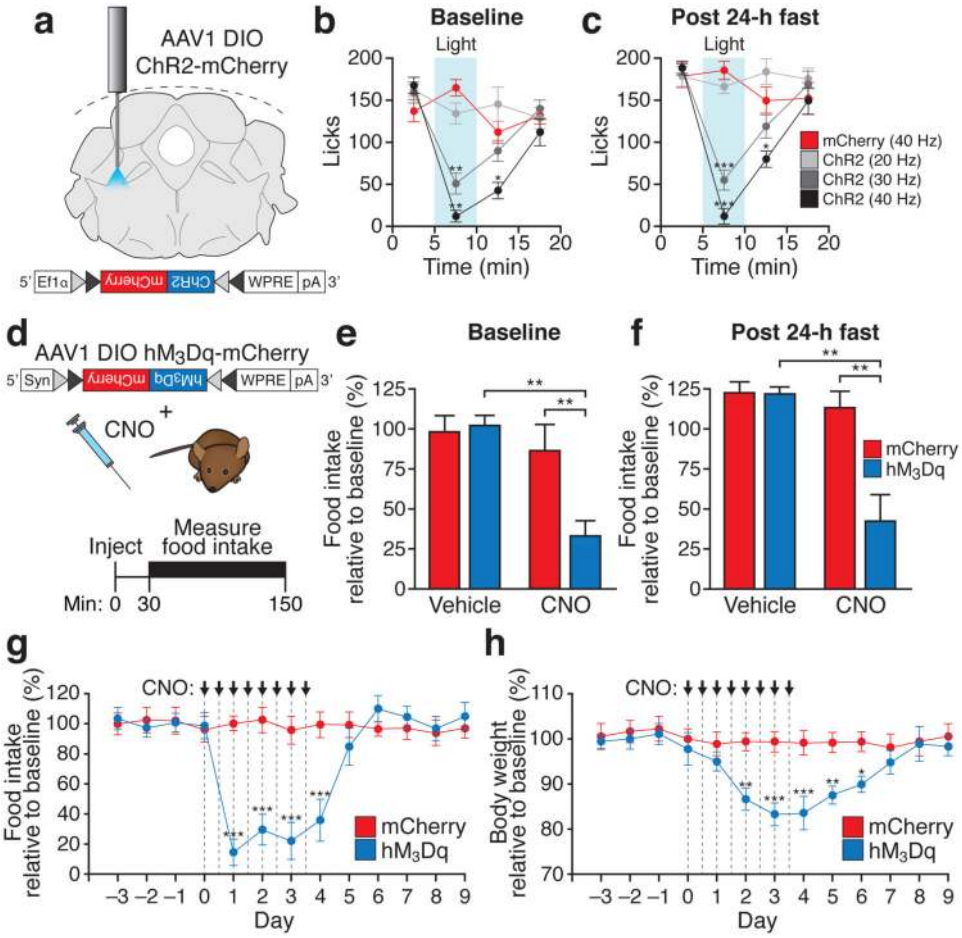

Figure 2. Stimulation of PBelo CGRP neurons reduces food intake and causes starvation

a, Placement of fiber optic implant in the PBN in a *Calca*$^{Cre/+}$ animal injected with AAV DIO ChR2-mCherry. **b, c,** Photostimulation of CGRP neurons reversibly inhibits food intake in both baseline (b) and fasted (c) conditions. **d,** Top, diagram showing AAV DIO hM$_3$Dq-mCherry transgene unilaterally injected into the PBN; bottom, timeline of experiments in (e-f). **e, f,** Pharmacogenetic stimulation of CGRP neurons inhibits food intake in both baseline (e) and fasted (f) conditions. **g, h,** Chronic administration of CNO (every 12 h for 4 d) suppresses food intake (g) and reduces body weight (h). *P<0.05, **P<0.01, ***P<0.001; See Supplementary Information for statistical analyses.

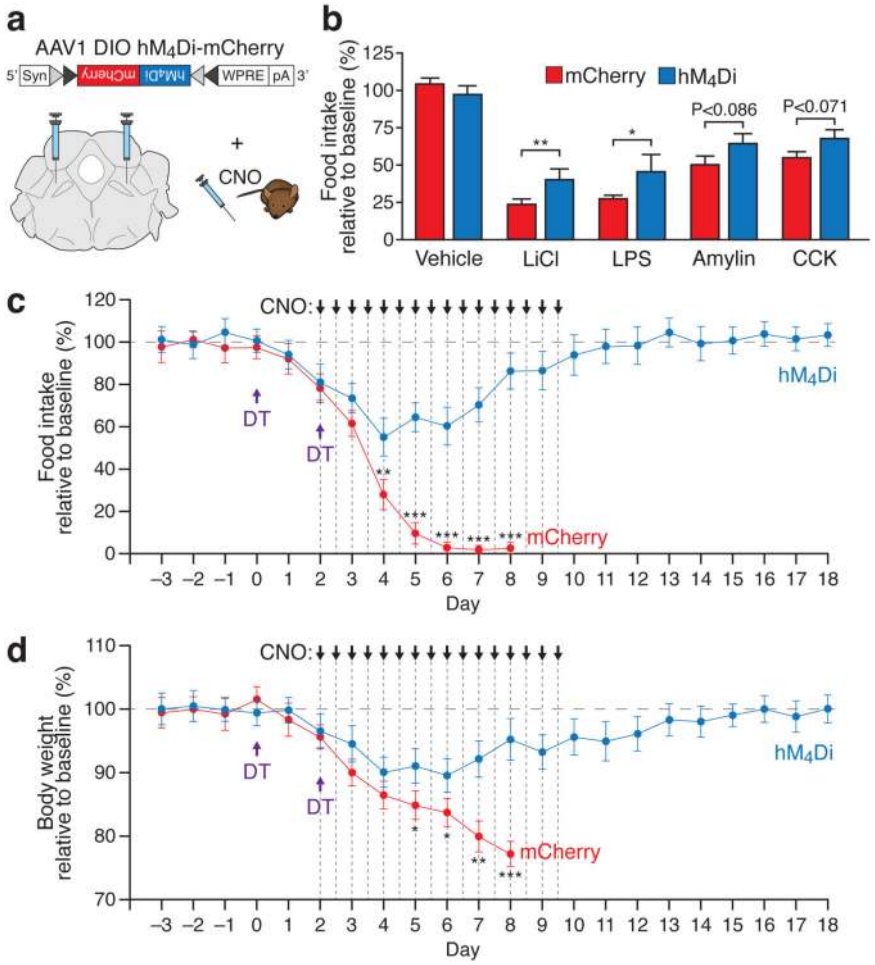

Figure 3. Inhibition of PBelo CGRP neurons increases food intake during conditions that suppress appetite

a, AAV DIO hM$_4$Di-mCherry transgene bilaterally injected into the PBN. **b,** Pharmacogenetic inhibition of CGRP neurons increases food intake after administration of anorexigenic compounds. **c, d,** Chronic administration of CNO (every 12 h for 8 d) increases food intake (c) and prevents starvation (d) in *Agrp*$^{DTR/+}$ mice after two injections of diphtheria toxin. The mCherry animals were sacrificed on day 8 due to extreme weight loss. *P<0.05, **P<0.01, ***P<0.001; see Supplementary Information for statistical analyses.

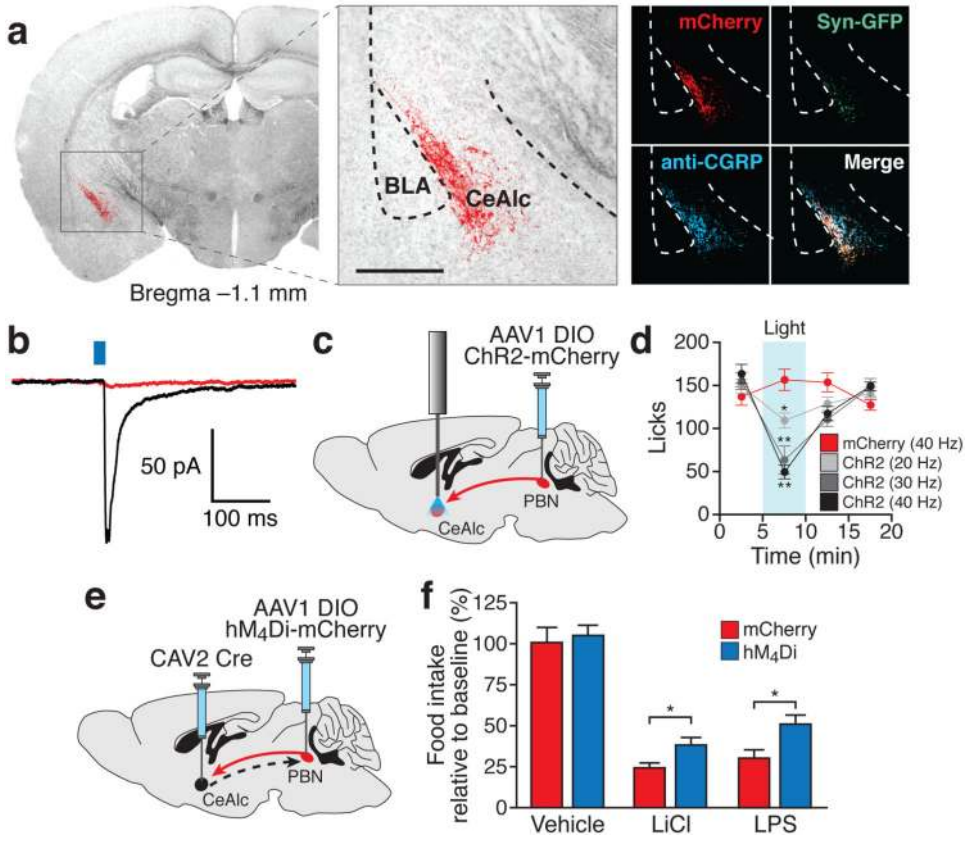

Figure 4. Efferent projections from PBelo CGRP neurons to the CeAlc mediate appetite suppression

a, Left and middle, mCherry-expressing fibers from the PBelo to the CeAlc; scale bar, 500 μm. Right, PBelo fibers expressing mCherry, Synaptophysin-GFP, and CGRP. **b,** EPSC from a CeAlc neuron upon photostimulation of PBelo-to-CeAlc fibers before (black) and after (red) bath application of CNQX and APV. **c,** AAV DIO ChR2-mCherry with fiber optic implant above the CeAlc. **d,** Photostimulation of PBelo fibers in the CeAlc reversibly inhibits food intake. **e**, Injection of CAV2 Cre into the CeAlc and AAV DIO hM_4Di-mCherry into the PBN. **f,** Inhibition of retrogradely-targeted PBelo neurons increases food intake. *P<0.05, **P<0.01; See Supplementary Information for statistical analyses.